Transverse Single-Spin Asymmetry for Very Forward Neutral Pion Production in Polarized $p + p$ Collisions at $\sqrt{s} = 510$ GeV

M. H. Kim[1,2] O. Adriani,[3,4] E. Berti,[3,4] L. Bonechi,[4] R. D'Alessandro,[3,4] Y. Goto,[2,5] B. Hong,[1] Y. Itow,[6,7] K. Kasahara,[8] J. H. Lee,[9] T. Ljubicic,[9] Y. Makino,[6] H. Menjo,[10] I. Nakagawa,[2,5] A. Ogawa,[9] J. S. Park,[2,11] T. Sako,[12] N. Sakurai,[13] K. Sato,[6] R. Seidl,[2,5] K. Tanida,[14] S. Torii,[15] A. Tricomi,[16,17,18] M. Ueno,[6] and Q. D. Zhou[6,*]

(RHICf Collaboration)

[1]*Korea University, Seoul 02841, Korea*
[2]*RIKEN Nishina Center for Accelerator-Based Science, Wako, Saitama 351-0198, Japan*
[3]*Department of Physics and Astronomy, University of Florence, Sesto Florentino (FI) I-50019, Italy*
[4]*INFN Section of Florence, Sesto Florentino (FI) I-50019, Italy*
[5]*RIKEN BNL Research Center, Brookhaven National Laboratory, Upton, New York 11973-5000, USA*
[6]*Institute for Space-Earth Environmental Research, Nagoya University, Nagoya, Aichi 464-8601, Japan*
[7]*Kobayashi-Maskawa Institute for the Origin of Particles and the Universe, Nagoya University, Nagoya, Aichi 464-8602, Japan*
[8]*Shibaura Institue of Technology, 307 Fukasaku, Minuma-ku, Saitama 337-8570, Japan*
[9]*Brookhaven National Laboratory, Upton, New York 11973-5000, USA*
[10]*Graduate school of Science, Nagoya University, Nagoya, Aichi 464-8601, Japan*
[11]*Department of Physics and Astronomy, Seoul National University, Seoul 08826, Korea*
[12]*Institute for Cosmic Ray Research, University of Tokyo, Kashiwa, Chiba 277-8582, Japan*
[13]*Tokushima University, Tokushima, Tokushima 770-8051, Japan*
[14]*Advanced Science Research Center, Japan Atomic Energy Agency, 21 2-4 Shirakata Shirane, Tokai-mura, Naka-gun, Ibaraki 319-1195, Japan*
[15]*RISE, Waseda University, Shinjuku, Tokyo 162-0044, Japan*
[16]*Department of Physics and Astronomy, University of Catania, Catania I-95123, Italy*
[17]*INFN Section of Catania, Catania I-95123, Italy*
[18]*CSFNSM, Catania I-95123, Italy*

Transverse single-spin asymmetries of very forward neutral pions generated in polarized $p + p$ collisions allow us to understand the production mechanism in terms of perturbative and nonperturbative strong interactions. During 2017, the RHICf Collaboration installed an electromagnetic calorimeter in the zero-degree region of the STAR detector at the Relativistic Heavy Ion Collider (RHIC) and measured neutral pions produced at pseudorapidity larger than 6 in polarized $p + p$ collisions at $\sqrt{s} = 510$ GeV. The large nonzero asymmetries increasing both in longitudinal momentum fraction x_F and transverse momentum p_T have been observed at low transverse momentum $p_T < 1$ GeV/c for the first time, at this collision energy. The asymmetries show an approximate x_F scaling in the p_T region where nonperturbative processes are expected to dominate. A non-negligible contribution from soft processes may be necessary to explain the nonzero neutral pion asymmetries.

Although the largest fraction of energy in high-energy hadronic collisions is concentrated in the very forward region, the reaction mechanism there is not well understood, yet. RHIC has an advantage to study the production

mechanism via the transverse single-spin asymmetry (A_N) of neutral particles in transversely polarized $p + p$ collisions. A_N is defined by $(d\sigma_{\text{left}} - d\sigma_{\text{right}})/(d\sigma_{\text{left}} + d\sigma_{\text{right}})$ or the corresponding azimuthal angular modulation where $\sigma_{\text{left (right)}}$ designates the particle production cross sections in the left (right) side of the polarization direction of the proton beam. Large values of A_N in hadron production have been measured in the forward pseudorapidity (η) region, $1 < \eta < 4$, in a wide range of collision energies [1–5].

These results have been explained by transverse momentum dependent (TMD) [6–8] and higher-twist functions

[9–11] in an initial or final state effect combined with the transverse motions of quarks and gluons. The TMD functions are used in describing Drell-Yan or weak boson production where the transverse momentum (p_T) and momentum transfer (Q^2) scales are observed. On the other hand, the higher-twist functions are used in inclusive hadron, photon, or jet production processes where only a single scale in p_T is observed.

Although large asymmetries could be explained by hard processes, recent measurements additionally suggest that they may originate from soft processes such as diffractive scattering. The AnDY experiment reported small A_N values in forward jet production, compared to that of forward hadron production [12]. The difference can be explained not only by the mixture and cancellation of u and d-quark jets, but potentially also by diffractive effects contributing to the hadron asymmetries.

The STAR experiment also reported, for π^0 production, a multiplicity dependence of A_N with the number of detected photons [13]. It showed that the A_N decreases as the event complexity increases and jetlike events show small asymmetries. This poses a question whether the large A_N values of π^0 are due to diffractive scattering. The present study investigates the asymmetries in the region where soft processes dominate by measuring A_N of π^0 at very forward rapidities and small p_T.

We installed the former LHCf Arm1 detector [14], now dubbed the RHICf detector, in front of one of the STAR zero-degree calorimeters (ZDC) [15], which was located 18 m away from the beam collision point, as shown in Fig. 1. At RHIC, the proton bunches rotating clockwise are referred to as "blue beam" and counterclockwise as "yellow beam". The RHICf detector is located in the downstream side of the blue beam. The zero-degree direction of the blue beam is also shown in Fig. 1. The RHICf detector consists of the two position-sensitive sampling calorimeters with square shape in the transverse plane, called TS (small

tower, with a 20 mm size) and TL (large tower, with a 40 mm size). Each detector consists of 17 tungsten absorbers with a total of 44 radiation lengths (or 1.6 nuclear interaction lengths), 16 sampling layers of GSO scintillators, and 4 X-Y pairs of the position layers with multianode photomultiplier tube readout. Each pair of position layers is composed of 20 (for TS) or 40 (for TL) 1-mm-wide GSO bars [16]. The RHICf detector has an energy resolution of 2%–3% and position resolution of 100–150 μm for 100–250 GeV photons. The two photons from π^0 decays can be detected in two different towers (type I) or within one tower (type II) [17]. For π^0's, the energy resolution at energies of 100–250 GeV is 2.5%–3.5% and the p_T resolution in $0.0 < p_T < 0.8$ GeV/c is 3.0%–4.5% for both types.

In order to cover a wide p_T range, the data were taken at three vertical positions of the detector where the beam enters (1) the center of the TL, (2) the center of the TS, and (3) 24 mm below the center of the TS. With these three configurations, we were able to measure A_N of the very forward π^0's at RHIC in $0.0 < p_T < 1.0$ GeV/c. The measured longitudinal momentum fraction (x_F) region was larger than 0.25. Further limits were imposed by the shadows of the upstream horizontal bending magnet, DX, and the beam pipe, resulting in the accepted pseudorapidity region of $\eta > 6$. Note that the current RHICf setup kinematically covers a lower p_T region than the PHENIX and STAR measurements, which is beneficial to studying the soft quantum chromodynamics (QCD) effects.

The RHIC proton beams are usually vertically polarized. 111 of 120 bunches are filled with beam spin orientation up or down in fixed bunch patterns. During the RHICf operation in 2017, the direction of the beam polarization was rotated by 90° by using the spin rotator magnets to radial polarization in order to reach maximal sensitivity of A_N and a maximal p_T range covered by the RHICf detector. The polarization ranged from 0.53 to 0.59 with a systematic uncertainty less than 0.02 [18]. The center-of-mass energy ($\sqrt{s}$) was 510 GeV with large β^* value of 8 m to make the angular beam divergence small. As a result, the luminosity of $\sim 10^{31}$ cm^{-2} s^{-1} in the RHICf operation was smaller than that in usual RHIC operation with a small β^*.

Three kinds of triggers were generally used for the neutral particle measurement. A shower trigger with a large prescale factor of < 30 was the baseline trigger. It required hits in three consecutive GSO sampling layers of the TS or TL tower. The type-I π^0 trigger was designed for the entire luminosity without any prescale factor. It required hits in the three consecutive layers in the upstream seven sampling layers of both TS and TL. Finally, the high-energy electromagnetic (high-EM) trigger was designed and optimized for the measurements of high-energy photons and type-II π^0's. It required a large energy deposit in the fourth sampling layer of the TS or TL, and was operated with a small prescale factor of ~ 2. In total, 1.1×10^8 events and an integrated luminosity of about 700 nb^{-1} were accumulated in 4 days of
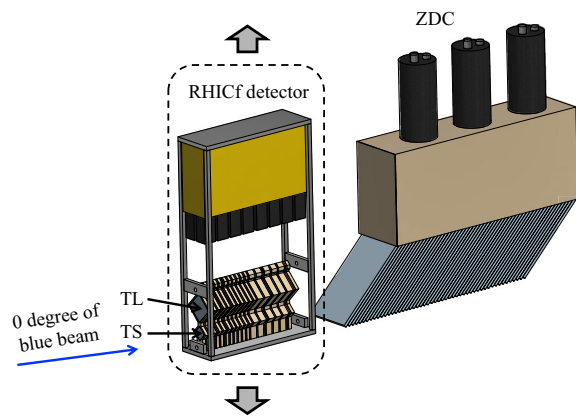

FIG. 1. Schematic drawing of the RHICf detector installed in front of the ZDC with the direction of the blue beam. We moved the detector vertically to cover p_T from 0.0 to 1.0 GeV/c.

the dedicated RHIC operation spanning about 28 h of data taking.

The hit positions of photons were estimated by fitting a Lorentzian-based function to the energy deposit distribution in the GSO bars. The photon energy was reconstructed based on the correlation between the energy deposit in the detector and its incident energy simulated by Geant4 [19]. The position dependent light collection efficiency and shower leakage effect were also considered for the reconstructed hit position. See Refs. [17,20] for more details on the correction procedure.

The photon events were separated from neutron background by requiring $8 < L_{90\%} < 18$, where $L_{90\%}$ is defined by the longitudinal depth for the measured energy deposition to reach 90% of the total. The rejection efficiencies for neutron and photon events with the above $L_{90\%}$ criterion are 99% and 4%, respectively, based on the QGSP-BERT4.0 model in Geant4. The neutron contamination in the π^0 sample was further suppressed to less than 0.1% by applying a two photon invariant mass cut which will be described later. Because of the poor energy and position resolutions, the photon hits in the DX magnet shadow region and the regions less than 2 mm from the detector edges were excluded in this analysis. The A_N distribution was analyzed as functions of x_F and p_T and the two-dimensional dependence was investigated. The boundaries of the x_F and p_T bins were determined in such a way that the A_N of all bins were not biased by specific detector position or the types of π^0.

For the forward single-spin asymmetry, only the polarization of the blue beam, the one moving toward the RHICf detector, is taken into account. On the other hand, for the backward asymmetry, where the sign of the x_F is reversed, only the polarization of the yellow beam is taken into account. The A_N value in each x_F and p_T bin was estimated by

$$A_N = \frac{1}{PD_\phi}\left(\frac{N_{\text{Left}} - RN_{\text{Right}}}{N_{\text{Left}} + RN_{\text{Right}}}\right), \qquad (1)$$

where P is the beam polarization, $N_{\text{Left(Right)}}$ is the number of detected π^0 in the left (right) side of the beam polarization direction, and R is the luminosity ratio of the spin orientations resulting into the events to right and left sides. The value of R, ranging from 0.958 to 0.995, was estimated using the charged particle rates tagged by the STAR beam beam counter [21] and vertex position detector [22]. The dilution of the asymmetry in azimuthal angle of π^0 was corrected using the dilution factor D_ϕ defined as

$$D_\phi = \sum_i \left(\frac{\sin\phi_i}{N}\right), \qquad (2)$$

where ϕ_i is the azimuthal angle of the π^0 with respect to the beam polarization direction in the ith event and the N is the number of π^0's detected. In this analysis, only type-I π^0

triggered events were used for the type-I analysis and high-EM triggered events for the type-II analysis before combining the asymmetries. In this way, the trigger efficiencies cancel in Eq. (1).

Values of A_N were corrected for the background contamination and the detector smearing effect. Figure 2 shows the reconstructed invariant mass distribution of the two photons and a clear π^0 peak at 135 MeV/c^2 is observed. Most of the background ($> 80\%$) comes from accidental coincidences between photons from different π^0's. Another major background is the combinatorial two particle background from direct photons, photons from η decays, and misidentified neutrons. According to the QGSJET II-04 model [23], the distribution near the peak is well described by the superposition of a Gaussian peak for the π^0 and sixth polynomial function for the background. The fitted functions and their sum are shown in Fig. 2. The width of 3σ around the peak position was chosen for the signal + background region, and the regions beyond 5σ to the left or right of the peak position were chosen as the pure background regions. The background-to-signal ratio N_B/N_S was estimated in the signal + background region. It decreases as x_F increases (54% at the lowest and 2% at the highest x_F bin) because higher-energy π^0's correspond to narrower opening angles, which reduces the acceptance of accidental coincidences.

The background asymmetries were subtracted by

$$A_N^S = \left(1 + \frac{N_B}{N_S}\right)A_N^{S+B} - \left(\frac{N_B}{N_S}\right)A_N^B, \qquad (3)$$

where A_N^{S+B}, A_N^S, and A_N^B are the estimated asymmetries in the signal + background, signal only, and background only, regions, respectively. According to the Monte Carlo simulation, the two photon invariant mass distribution has a small tail in the lower mass region due to the underestimated reconstruction energy in a few events. A small fraction ($\sim 4\%$) of real π^0 events in the background region
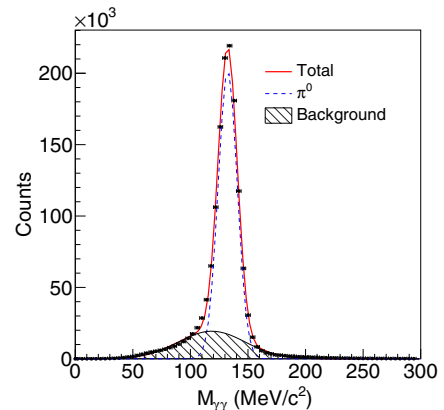

FIG. 2. Reconstructed two photon invariant mass distribution of type I in $x_F > 0.25$ and $0.0 < p_T < 1.0$ GeV/c.

contributes to this tail and the actual N_B/N_S can be smaller than the one estimated by the fitting, due to these π^0 events. Because the probability of the underestimated reconstruction energy increases when the photon hit approaches the edge of the tower, an even larger area along the edge than the one applied for π^0, with a width of 4 mm, was excluded for the background estimation. With this condition, the π^0 tail in the background region almost disappears ($< 0.05\%$). All background asymmetries were consistent with zero within the statistical uncertainties. The variation of A_N for the π^0 distributions with and without the tail was considered as one of the systematic uncertainties. The typical size of this uncertainty is ~ 0.0003.

For additional sources of the systematic uncertainty, the variation in the beam center position and the smearing effect for x_F and p_T were considered. The beam center is obtained by extrapolating the direction of the blue beam to the detector as follows. In the first method, the high-energy neutron hit distribution was fitted by a two-dimensional Gaussian function. In the second method, the neutron asymmetries were scanned as a function of their mean vertical position by using the fact that very forward neutrons have zero asymmetry at the vertical position of the beam center [24]. The difference of the two determined beam centers was less than 1.3 mm and the corresponding systematic uncertainty was 0.0003–0.0089 depending on x_F and p_T, which is assigned to the systematic uncertainty of A_N.

The effect of smearing due to the resolutions of x_F and p_T was studied in detail with Geant4. The dependence of π^0 asymmetries on x_F and p_T were artificially generated using weights. Single π^0's were generated considering the detection efficiencies matching the reconstructed energy and p_T distributions of the data. The simulation was tuned to the data for the beam profile, detector noise, signal attenuation, and measured fluctuations including the cross talk effect in the GSO bars described in Ref. [25]. The data analysis code was also used in the simulation for the reconstruction of π^0's and the calculation of the asymmetry. The contamination level defined by the ratio of the incorrectly and the legitimately reconstructed events in a given (x_F, p_T) bin was estimated in the simulation, where the reconstructed x_F and p_T values of the incorrect events were out of the range for the bin where the true values belong to. The contamination level for type-I and type-II π^0 are all less than 35%, and more than 90% of the migrated events are from $\delta x_F < 0.025$ and $\delta p_T < 0.035$ GeV/c of the bin boundaries. The differences between the reconstructed and true $\langle x_F \rangle$, $\langle p_T \rangle$, and A_N values of each bin due to smearing are less than 0.008, 0.009 GeV/c, and 0.0015, respectively, which are negligible. This result is in agreement with our expectations because the resolutions of x_F and p_T of the detector are much smaller than the bin sizes.

Furthermore, to find any missing systematic effects having not been considered, a "bunch shuffling" analysis was performed by randomly reassigning bunch numbers given for a given polarization pattern. Ideally, the calculated asymmetries and their fluctuations after the bunch shuffling should be centered around zero with a width which is given by the statistical uncertainties of the asymmetries. The bunch shuffled asymmetries were consistent with zero with fluctuation comparable to statistical uncertainties. Therefore, we conclude that there are no noticeable false asymmetries introduced in the experiment and analysis.

Figure 3 and Table I summarize the A_N values of very forward π^0's as functions of x_F and p_T. In addition to the systematic effects described above, additional systematic uncertainties of 0.0005–0.0092 were caused by the variation of the determined beam polarization. Because all discussed systematic uncertainties are independent, the quadratic sums of them are considered as the total systematic uncertainties. The uncertainties of the dilution factors are not included because its magnitude is less than 0.0001.

Figure 3(a) shows that A_N of the very forward π^0's increases with p_T, reaching about 0.2 at ~ 0.8 GeV/c, where the production mechanism is mainly governed by
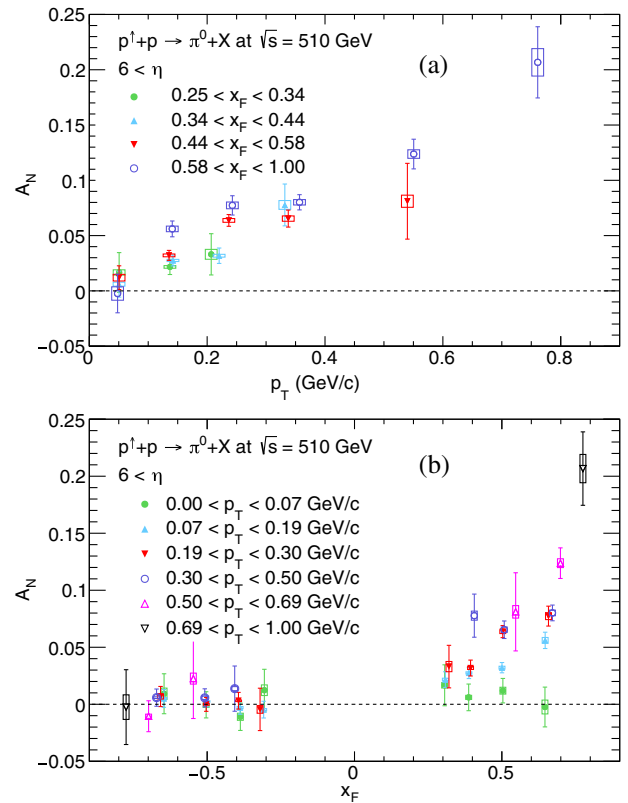

FIG. 3. A_N of the very forward π^0's as functions of (a) p_T for several x_F ranges and (b) x_F for several p_T ranges. Only forward A_N was presented in (a). Error bars represent the statistical uncertainties, and the boxes represent the systematic uncertainties.

TABLE I. A_N of very forward π^0's as a function of $\langle x_F \rangle$ and $\langle p_T \rangle$.

$\langle x_F \rangle$	$\langle p_T \rangle$ (GeV/c)	A_N	Statistical uncertainty	Systematic uncertainty			
				Total	Beam center	Polarization	Background
−0.79	0.77	0.0025	0.0328	0.0108	0.0107	0.0001	0.0009
−0.70	0.55	0.0105	0.0136	0.0018	0.0017	0.0004	0.0001
−0.68	0.37	−0.0058	0.0076	0.0007	0.0006	0.0003	0.0000
−0.66	0.24	−0.0068	0.0088	0.0022	0.0021	0.0002	0.0000
−0.66	0.15	−0.0051	0.0078	0.0008	0.0007	0.0002	0.0000
−0.64	0.04	−0.0092	0.0175	0.0050	0.0049	0.0009	0.0001
−0.54	0.53	−0.0225	0.0350	0.0048	0.0044	0.0020	0.0004
−0.52	0.34	−0.0056	0.0079	0.0014	0.0012	0.0006	0.0004
−0.50	0.23	0.0001	0.0061	0.0007	0.0006	0.0001	0.0002
−0.51	0.14	−0.0025	0.0047	0.0006	0.0005	0.0001	0.0003
−0.50	0.04	0.0004	0.0108	0.0023	0.0022	0.0001	0.0003
−0.41	0.33	−0.0137	0.0198	0.0018	0.0016	0.0006	0.0001
−0.39	0.23	−0.0031	0.0073	0.0007	0.0005	0.0004	0.0003
−0.39	0.14	0.0030	0.0058	0.0009	0.0007	0.0003	0.0004
−0.38	0.06	0.0109	0.0120	0.0031	0.0027	0.0012	0.0007
−0.31	0.21	0.0045	0.0186	0.0034	0.0033	0.0006	0.0003
−0.31	0.13	0.0047	0.0073	0.0009	0.0009	0.0003	0.0001
−0.30	0.04	−0.0123	0.0181	0.0047	0.0045	0.0009	0.0009
0.30	0.04	0.0167	0.0179	0.0024	0.0023	0.0005	0.0004
0.31	0.13	0.0217	0.0068	0.0011	0.0010	0.0006	0.0000
0.31	0.21	0.0331	0.0186	0.0044	0.0043	0.0010	0.0002
0.38	0.06	0.0061	0.0116	0.0017	0.0015	0.0010	0.0001
0.39	0.14	0.0275	0.0049	0.0009	0.0003	0.0009	0.0002
0.39	0.23	0.0318	0.0069	0.0012	0.0006	0.0010	0.0003
0.41	0.33	0.0777	0.0189	0.0039	0.0019	0.0035	0.0002
0.50	0.04	0.0119	0.0107	0.0030	0.0029	0.0007	0.0001
0.51	0.14	0.0321	0.0045	0.0013	0.0007	0.0011	0.0000
0.50	0.23	0.0637	0.0053	0.0017	0.0006	0.0016	0.0001
0.52	0.34	0.0654	0.0076	0.0024	0.0017	0.0017	0.0002
0.54	0.53	0.0811	0.0342	0.0054	0.0040	0.0036	0.0006
0.64	0.04	−0.0024	0.0174	0.0061	0.0060	0.0007	0.0000
0.66	0.15	0.0561	0.0071	0.0025	0.0014	0.0021	0.0001
0.66	0.24	0.0773	0.0087	0.0030	0.0018	0.0024	0.0001
0.68	0.37	0.0801	0.0068	0.0024	0.0011	0.0022	0.0002
0.70	0.55	0.1237	0.0134	0.0038	0.0012	0.0036	0.0004
0.79	0.77	0.2067	0.0321	0.0124	0.0081	0.0092	0.0019

nonperturbative QCD. Figure 3(b) shows that the backward A_N distributions are consistent with zero. Similarly, the forward A_N is consistent with zero in $p_T < 0.07$ GeV/c, but it starts to increase as a function of x_F at higher p_T. The comparison with the previous forward π^0 measurements is depicted in Fig. 4 [26–28]. It shows that the increasing trend of the very forward π^0 asymmetry is comparable to the previous measurements at higher p_T regions from FNAL and RHIC, that were successfully described by hard processes for the π^0 production in polarized $p + p$ collisions [11]. The current results are the first measurement showing the onset of the rising asymmetry at $p_T \lesssim 1$ GeV/c at RHIC energy. The present data, with the previous STAR data [13], raise the interesting question on the relation between the soft and hard process contributions for A_N of π^0's. The same question also applies to the similar x_F scaling phenomenon for the charged pion asymmetries at lower $\sqrt{s}$ of ZGS [29] and AGS [30] and that at higher $\sqrt{s}$ of FNAL and RHIC. To answer this question, it would be desirable to investigate the same observables in the unexplored kinematic region between the low and high p_T values of 0.8–2.0 GeV/c.

A clear nonzero A_N in the RHICf data at low p_T, and the same x_F scaling with the previous measurements for forward π^0's, indicates that diffractive processes may also contribute to the asymmetries at higher p_T, where hard
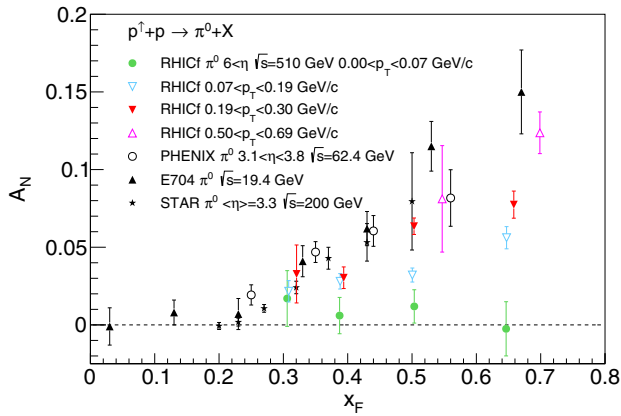
FIG. 4. Comparison of the RHICf data with the previously measured A_N of the forward π^0's as a function of x_F.

processes are expected to be dominant. For more detailed studies, STAR's central detectors and Roman pots [31] will be helpful to understand the mechanism for the π^0 asymmetries and the relative contributions of soft and hard processes.

In summary, the single-spin asymmetries of very forward π^0's have been measured by the RHICf detector at the zero-degree area of the STAR detector at RHIC in polarized $p + p$ collisions at $\sqrt{s} = 510$ GeV. Large A_N values up to ~ 0.2 were observed in the very forward region for $p_T < 0.8$ GeV/c. Empirical x_F scaling was also observed in $p_T > 0.19$ GeV/c, which is similar to the data in the higher p_T region.

---

[*]Present address: Institute of Particle and Nuclear Studies, High Energy Accelerator Research Organization (KEK), Tsukuba, Ibaraki 305-0801, Japan.

[1] A. Adare *et al.* (PHENIX Collaboration), Phys. Rev. D **90**, 012006 (2014).
[2] B. I. Abelev *et al.* (STAR Collaboration), Phys. Rev. Lett. **101**, 222001 (2008).
[3] D. L. Adams *et al.* (E581 and E704 Collaborations), Phys. Lett. B **261**, 201 (1991).
[4] B. E. Bonner *et al.*, Phys. Rev. Lett. **61**, 1918 (1988).
[5] R. D. Klem *et al.*, Phys. Rev. Lett. **36**, 929 (1976).
[6] D. W. Sivers, Phys. Rev. D **41**, 83 (1990).
[7] J. C. Collins, Nucl. Phys. **B396**, 161 (1993).
[8] J. C. Collins, S. F. Heppelmann, and G. A. Ladinsky, Nucl. Phys. **B420**, 565 (1994).
[9] J. W. Qiu and G. F. Sterman, Nucl. Phys. **B378**, 52 (1992).
[10] H. Eguchi, Y. Koike, and K. Tanaka, Nucl. Phys. **B763**, 198 (2007).
[11] K. Kanazawa, Y. Koike, A. Metz, and D. Pitonyak, Phys. Rev. D **89**, 111501(R) (2014).
[12] L. C. Bland *et al.* (AnDY Collaboration), Phys. Lett. B **750**, 660 (2015).
[13] M. M. Mondal *et al.* (STAR Collaboration), Proc. Sci., DIS2014 (**2014**) 216.
[14] O. Adriani *et al.* (LHCf Collaboration), Phys. Rev. D **94**, 032007 (2016).
[15] C. Adler, A. Denisov, E. Garcia, M. Murray, H. Stroebele, and S. White, Nucl. Instrum. Methods Phys. Res., Sect. A **470**, 488 (2001).
[16] T. Suzuki, K. Kasahara, K. Kawade, T. Murakami, K. Masuda, T. Sako, and S. Torii, J. Instrum. **8**, T01007 (2013).
[17] O. Adriani *et al.* (LHCf Collaboration), Phys. Rev. D **94**, 032007 (2016).
[18] RHIC p-Carbon Measurements, https://www.phy.bnl.gov/cnipol/rundb/.
[19] S. Agostinelli *et al.* The Geant4 Collaboration, Nucl. Instrum. Methods **506**, 250 (2003).
[20] O. Adriani *et al.* (LHCf Collaboration), Phys. Lett. B **703**, 128 (2011).
[21] C. A. Whitten, Jr. *et al.* (STAR Collaboration), The beam-beam counter: A local polarimeter at STAR, https://www.star.bnl.gov/eca/LocalPol/BBCproceeding-Chuck.pdf.
[22] W. J. Llope *et al.*, Nucl. Instrum. Methods Phys. Res., Sect. A **759**, 23 (2014).
[23] S. Ostapchenko, Nucl. Phys. B, Proc. Suppl. **151**, 143 (2006).
[24] A. Adare *et al.* (PHENIX Collaboration), Phys. Rev. D **88**, 032006 (2013).
[25] Y. Makino *et al.* (LHCf Collaboration), J. Instrum. **12**, P03023 (2017).
[26] D. L. Adams *et al.* (FNAL-E581 and E704 Collaborations), Phys. Lett. B **261**, 201 (1991).
[27] A. Adare *et al.* (PHENIX Collaboration), Phys. Rev. D **90**, 012006 (2014).
[28] B. I. Abelev *et al.* (STAR Collaboration), Phys. Rev. Lett. **101**, 222001 (2008).
[29] R. D. Kelm, J. E. Bowers, H. W. Courant, H. Kagan, M. L. Marshak, E. A. Peterson, K. Ruddick, W. H. Dragoset, and J. B. Roberts, Phys. Rev. Lett. **36**, 929 (1976).
[30] C. E. Allgower *et al.* (E925 Collaboration), Phys. Rev. D **65**, 092008 (2002).
[31] S. Bültmann *et al.*, Nucl. Instrum. Methods A **535**, 415 (2004).

Correction: A third affiliation has been added for the 23rd author.